Building on the Strengths of a Double-Hybrid Density Functional for Excitation Energies and Inverted Singlet-Triplet Energy Gaps

Kevin Curtis,[1] Olajumoke Adeyiga,[1] Olabisi Suleiman,[1] Samuel O. Odoh*,[1]

AFFILIATIONS

Department of Chemistry, University of Nevada, Reno, NV 89557

a) Author to whom correspondence should be addressed: sodoh@unr.edu
b) Electronic mail: sodoh@unr.edu

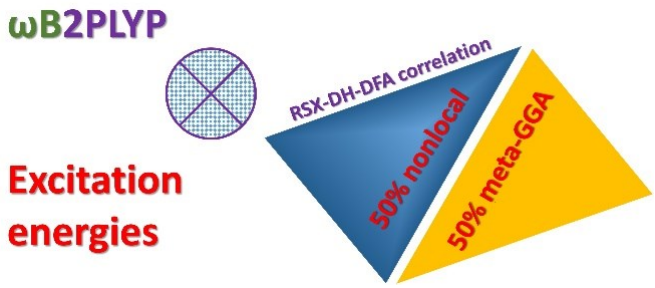

ABSTRACT: It is demonstrated that a double hybrid density functional approximation (DH-DFA), ωB88PTPSS, that incorporates equipartition of density functional theory (DFT) and non-local correlation however with a meta-GGA correlation functional as well as with the range-separated exchange of ωB2PLYP provides accurate excitation energies for conventional systems as well as correct prescription of negative singlet-triplet gaps for non-conventional systems with inverted gaps, without any necessity for parametric scaling of the same-spin and opposite-spin non-local correlation energies. Examined over "*safe*" excitations of the QUESTDB set, ωB88PTPSS performs quite well for open-shell systems, correctly and fairly accurately (relative to EOM-CCSD reference) predicts negative gaps for 50 systems with inverted singlet-triplet gaps, is one of the leading performers for intramolecular charge-transfer excitations and achieves near-CC2 and ADC(2) quality for the Q1 and Q2 subsets. Subsequently, we tested ωB88PTPSS on two sets of *real-life* examples from recent computational chemistry literature; the low energy bands of chlorophyll *a* (Chl *a*) and a set of thermally activated delayed fluorescence (TADF) systems. For Chl *a*, ωB88PTPSS quantitatively and quantitatively achieves DLPNO-STEOM-CCSD-level performance and provides excellent agreement with experiment. For TADF systems, ωB88PTPSS agrees quite well with SCS-CC2 excitation energies as well as experimental values for the gaps between the S_1 and T_1 excited states.

1. INTRODUCTION

Density Functional Theory (DFT) is the most widely used quantum-mechanical approach for studying ground state properties and reactions; due to its good accuracy-to-computational cost ratio. However, DFT results can be very sensitive to the choice of exchange-correlation density functional. This has motivated many extensive benchmark studies to establish suitability of various density functionals for various classes of systems and properties. Time-dependent DFT, TD-DFT[1-4], the extension of DFT for excited state properties, has also garnered widespread use. TD-DFT, commonly used with the linear-response formalism[5] and adiabatic approximation, also suffers from dependence on choice of density functional. Thus, there have been many efforts towards developing modern density functional approximations (DFAs) with improved accuracy and broader applicability. There have been semiempirical DFAs fitted to actual or computed data for real systems, as well as non-empirical functionals designed to satisfy some constraints, without fitting to data for real systems. Additionally, there have been efforts to compile datasets/databases with highly accurate experimental or theoretical data, useful for rigorous benchmarking of the performance of newer and extant DFT functionals. For example, the QUESTDB set contains highly accurate vertical excitation energies, useful for evaluating the performance of DFAs employed in linear-response TD-DFT.[6] For TD-DFT, double-hybrid DFAs (DH-DFAs) have become particularly useful for studying excited state properties.[7-10] These DH-DFAs use perturbative corrections from second-order Møller-Plesset perturbation (MP2) theory[11-13] to correct the ground state total energy.[14, 15]

$$E_{\mathrm{xc}}^{\mathrm{DH-DFA}} = (1-a_x)E_{\mathrm{x}}^{\mathrm{DFT}} + a_x E_{\mathrm{x}}^{\mathrm{HF}} + (1-a_c)E_{\mathrm{c}}^{\mathrm{DFT}} + a_c E_{\mathrm{c}}^{\mathrm{MP2}}$$

Here, $E_{\mathrm{x}}^{\mathrm{DFT}}$ and $E_{\mathrm{x}}^{\mathrm{HF}}$ depict contributions to the exchange energy from DFT and Hartree-Fock theory, respectively, while $E_{\mathrm{c}}^{\mathrm{DFT}}$ and $E_{\mathrm{c}}^{\mathrm{MP2}}$ respectively, depict contributions to the correlation energy from a correlation density functional and MP2. Grimme and Neese showed that corrections from the configurations interactions singles with perturbative doubles, CIS(D), method[16] are required for the total energies of the excited states,[17] allowing one to generalize:

$$E_{\mathrm{xc}}^{\mathrm{DH-DFA}} = (1-a_x)E_{\mathrm{x}}^{\mathrm{DFT}} + a_x E_{\mathrm{x}}^{\mathrm{HF}} + (1-a_c)E_{\mathrm{c}}^{\mathrm{DFT}} + a_c E_{\mathrm{c}}^{\mathrm{nonlocal}}$$

and formulate that the excitation energy from the DH-DFA, $\omega_{\mathrm{DH-DFA}}$, as the sum of the excitation energy from the DFA with truncated correlation, ω, and a perturbative doubles correction from CIS(D), $\Delta_{(\mathrm{D})}$, scaled by a_c, the coefficient of the MP2 correlation for ground state energies.[17]

$$\omega_{\mathrm{DH-DFA}} = \omega + a_c\Delta_{(\mathrm{D})}$$

The mixing ratios of the exchange and correlation components of DH-DFAs have been determined via parameteriz-ation (semiempirical) or via recourse to theoretical constraints and/or arguments (nonempirical). However, semiempirical DH-DFAs are not less accurate as a result of their construction. Notably, several studies have shown semiempirical DH-DFAs to be more accurate than non-empirical ones.[18-22]

Overall, the sub-field of DH-DFA development focused on predicting excitation energies is a growing and exciting field. As an example, to improve applicability of DH-DFAs to charge-transfer excitations, there has been great progress in development of range-separated (long-range corrected, (LC-) DH-DFAs. These LC- DH-DFAs combine the earlier tradition of LC hybrid functionals with DH-DFAs.[23-26] In these, the electron-repulsion operator is decomposed into two regimes, short-range (SR) and long-range (LR), with an error function allowing dampened SR DFT exchange to be supplemented with Hartree-Fock exchange, with the latter also ensuring a correct description of the asymptotic tail of the exchange-correlation potential in the LR. A prominent example of the LC-DH-DFAs is the ωB2PLYP functional of Casanova-Paez et al.,[27] which has shown good performance for the excited-states of a wide variety of systems. Some of us have used this functional to study the excited state properties of copper-oxo clusters embedded in zeolite catalysts.[28-30] The energy expression for ωB2PLYP is

$$E_{\mathrm{xc}}^{\omega\mathrm{B2PLYP}} = 0.47E_{\mathrm{x}}^{\omega\mathrm{B88}}(\omega) + 0.53E_{\mathrm{x}}^{\mathrm{SR-HF}} + E_{\mathrm{x}}^{\mathrm{LR-HF}} + 0.73E_{\mathrm{c}}^{\mathrm{LYP}} + 0.27E_{\mathrm{c}}^{\mathrm{nonlocal}}$$

For ωB2PLYP, the range-separation parameter, ω, is 0.30 bohr^{-1}, which as noted damps the DFT exchange, $E_{\mathrm{x}}^{\omega\mathrm{B88}}$, in the LR to be replaced by Hartree-Fock exchange, $E_{\mathrm{x}}^{\mathrm{LR-HF}}$, and in the SR to be combined with it thereof, $E_{\mathrm{x}}^{\mathrm{SR-HF}}$. The DFT contribution to the exchange is a generalized gradient approximation (GGA), B88.[31] Likewise, the DFT contribution to the correlation is LYP, a GGA correlation functional.[32]

Given our previous use of ωB2PLYP, we are interested in ongoing evaluations of its performance as well as development of similar DFAs by other workers. However, it was recently reported that ωB2PLYP, and many other DH-DFAs lead to positive energy gaps for many systems with inverted singlet-triplet (IST) gaps.[33] These organic systems are useful for making organic light emitting diodes (OLEDs) for display and lighting applications. They are similar to previously described thermally activated delayed fluorescence (TADF) and multi-resonant TADF (MR-TADF) materials which possess small gaps between the first singlet, S_1, and triplet excited, T_1, states, ΔE_{S1T1}. However, unlike TADF and MR-TADF emissive materials, systems with IST gaps violate Hund's multiplicity rule via an inversion of the lowest S_1, and T_1. Inversion of the ΔE_{S1T1} gap replaces up-conversion of TADF and MR-TADF emitters with down-conversion, leading to improved material stability and internal quantum efficiency. An earlier study by Rodrigo et al. reported that strong correlation effects beyond the ability of TDA-DFT are responsible for inversion of the ΔE_{S1T1} gaps in several triangulene-like molecules.[34] Sancho-Garcia et al. provided recommendations on choosing DH-DFAs for studying such inversions.[35] Alipour and Izadkhast showed that scaling of the same-spin (SS) and opposite-spin (OS) components of MP2 as well as the direct and indirect terms of CIS(D) correlation energies are needed to capture the negative energy gaps of organic emissive materials with IST gaps.[33] Two of these DH-DFAs are SOS0-CIS(D)-RSX-PBE0-DH and SOS0-CIS(D)-PBE0-DH, with RSX indicating the functional uses range-separated exchange. Although these new DH-DFAs accurately predict negative energy gaps for the IST systems, their performances for the excited state properties of conventional systems remain unknown. It is also interesting to consider whether accurate descriptions of the IST systems can be achieved without SS and OS scaling. Alipour and Izadkast compared the SOS0-CIS(D) and SOS0-CIS(D)-RSX functionals to many "conventional" DH-DFAs.[33] One of the DH-DFAs with moderately good performance is PBE0-2[36] which has an equal partition of DFT and non-local correlation with the energy expression

$$E_{\mathrm{xc}}^{\mathrm{PBE0-2}} = 0.2063E_{\mathrm{x}}^{\mathrm{PBE}} + 0.7937E_{\mathrm{x}}^{\mathrm{HF}} + 0.5E_{\mathrm{c}}^{\mathrm{DFT}} + 0.5E_{\mathrm{c}}^{\mathrm{nonlocal}}$$

Out of 50 IST systems, PBE0-2 correctly predicts negative gaps for 48, boasting a mean signed error, MSE, of 0.01 eV from reference values of the singlet-triplet gaps. Its mean absolute error, MAE, was 0.03 eV and it had a root mean squared error, RMSE,

of 0.04 eV. For perspective, the best performing SOS0-CIS(D)-PBE-QIDH DFA has MSE, MAE and RMSE of -0.02, 0.02 and 0.03 eV, respectively.[33] However, PBE0-2 has a reduced predictive value as it yields positive energy gaps for some IST systems. In summary, previous works show that while ωB2PLYP is very useful for conventional open-shell systems, it fails dramatically for IST species.[18, 27-30, 33, 37, 38] However, PBE0-2 is better, albeit imperfect, for IST species but performs poorly for doublet-doublet excitations. Moreover, PBE0-2 performs well for many conventional systems.[38] These results suggest that a DH-DFA that combines the strengths of ωB2PLYP and PBE0-2 might have improved applicability over conventional and IST systems. However Alipour and Izadkast tested the RSX-PBE0-2 functional[39] for IST systems, finding that it yields 17 positive energy gaps, out of 50.[33] Thus, range-separation of the exchange is not necessarily enough to correctly describe IST systems while retaining accuracy for conventional systems. On the other hand, Peverati and Truhlar demonstrated that the accuracy of hybrid meta-GGAs can be improved with range separation.[40] They found with their M11 functional, improved accuracies for ground- and excited-state properties. In this work, we are mostly interested in computing excitation energies and the singlet-triplet gaps of IST systems, with ωB2PLYP and PBE0-2 as starting points. Thus, we define the ωB88PTPSS functional as

$$E_{\mathrm{xc}}^{\omega\mathrm{B88PTPSS}} = 0.47E_{\mathrm{x}}^{\omega\mathrm{B88}}(\omega) + 0.53E_{\mathrm{x}}^{\mathrm{SR-HF}} + E_{\mathrm{x}}^{\mathrm{LR-HF}} + 0.5E_{\mathrm{c}}^{\mathrm{TPSS}} + 0.5E_{\mathrm{c}}^{\mathrm{nonlocal}}$$

This functional contains an equipartition of DFT and nonlocal correlation, like PBE0-2.[36] Notice however that the DFT correlation is provided by the nonempirical TPSS meta-GGA functional.[41] The exchange is the same as for ωB2PLYP, with ω also being 0.30 bohr^{-1}.[27] To the best of our knowledge, there doesn't appear to be any formal requirement for the exchange and correlation functionals to belong to the same rung of the "Jacob's ladder" of DFAs.[42] Moreover, one could certainly describe a modified version of ωB2PLYP with equipartition of the correlation energy

$$E_{\mathrm{xc}}^{\omega\mathrm{B2PLYP-50\%}} = 0.47E_{\mathrm{x}}^{\omega\mathrm{B88}}(\omega) + 0.53E_{\mathrm{x}}^{\mathrm{SR-HF}} + E_{\mathrm{x}}^{\mathrm{LR-HF}} + 0.50E_{\mathrm{c}}^{\mathrm{LYP}} + 0.50E_{\mathrm{c}}^{\mathrm{nonlocal}}$$

However, tests on ethylene as well as the vinyl and hydroxyl radicals revealed that excitation energies from ωB2PLYP-50% tracked closer to ωB2PLYP than ωB88PTPSS. As a disparate example, the charge-transfer excitation of hydrogen chloride, HCl, is predicted by ωB2PLYP-50% to be at 7.66 eV, quite far from the TBE of 7.84 eV. For this excitation, ωB88PTPSS yields a value of 7.81 eV and ωB2PLYP gives 7.82 eV. We thus decided to proceed with ωB88PTPSS, hypothesizing that using meta-GGA correlation could help regularize Kohn-Sham orbitals and orbital eigenvalues obtained with damped DFT correlation.[43] Moreover, Santra et al. reported that for ground state energies, the same-spin correlation component could be eliminated by involving SCAN[44] nonempirical meta-GGA as the semilocal component.[45] There is earlier work on double hybrids with meta-GGAs by Souvi et al.[46]. Also, ωB88PTPSS is a good starting point for including RS meta-GGA exchange while seeking a LC-DH-DFA with minimal number of parameters. However, there are already other meta-GGA DH-DFAs in the literature.[47, 48] In any case, the very popular ωB97M(2) functional uses the xDH[49] approach, making computing excitation energies cumbersome.[50] There are also other DH-DFAs, like SCAN0-2, with 50% MP2 correlation.[51] Notice that by altering the correlation of ωB2PLYP, we are likely sacrificing situations where excitation energies are very sensitive to nonlocal corrections.[19, 52] Thus, a broad evaluation of ωB88PTPSS' performance for excitation energies and ΔE_{S1T1} gaps is needed.

2. COMPUTATIONAL DETAILS

2.1 Systems of Interest: A summary of the systems examined in this work is provided in Scheme 1.

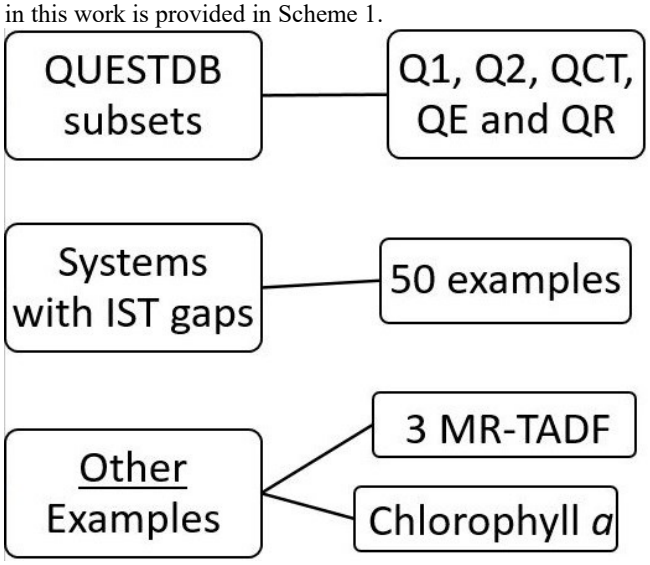

Scheme 1. Summary of systems considered in this work.

We first performed TDA-DFT calculations on five subsets of the QUESTDB excitation energy set. These excitation energies and systems were selected by Liang et al. and are considered safe for linear-response TDA-DFT calculations.[53] The subsets selected by Liang et al. are QR (open-shell systems), QCT (intramolecular charge-transfer excitations), QE (exotic systems), Q1 and Q2.[53] Additional descriptions of these subsets are provided below.

For the second set, we performed TDA-DFT calculations on the 50 systems with inverted ΔE_{S1T1} gaps examined previously.[33] Lastly, we considered the low-energy excitations of chlorophyll *a* (Chl *a*)[54] and a set of large organic MR-TADF emitters.[55] The former is important to understanding of biological photochemistry, while the latter are important for optimizing next-generation materials. Chl *a* was studied with TD-DFT while the MR-TADF species were studied with TDA-DFT. With these choices, we are able to compare our results to those reported previously in the literature.

2.2 Basis Sets: All TD-DFT and TDA-DFT calculations on subsets of the QUESTDB set were performed with triple-ζ aug-cc-pVTZ basis sets.[56-58] For the 50 systems with IST gaps as well as chlorophyll *a*, we used def2-TZVP basis sets.[59] For the MR-TADF emitters, we used 6-31G(d,p) basis sets.

2.3 Geometries: The QUESTDB set contains previously-optimized geometries for every compound. These geometries were used as is. For the 50 systems with IST gaps, geometry optimizations were performed at the B3LYP-D3BJ/def2-TZVP[32, 60-64] level. Optimized geometries were confirmed as local minima by performing vibrational frequency analyses. For chlorophyll *a*, we used the geometry optimized at the CAM-B3LYP/def2-TZVP level by Sirohiwal et al.[54] For MR-TADF systems, we used geometries optimized at the SCS-CC2 level previously by Hall et al.[55]

2.4 Software: All calculations with ωB88PTPSS were performed with the Q-Chem software suite, version 5.4.1.[65] All other calculations were performed with ORCA code, version 5.0.3.[66, 67] All calculations in the ORCA code were performed

with def-grid3 and sped up with the resolution-of-the-identity for Coulomb integrals and the numerical chain-of-sphere integration for Hartree-Fock exchange, RIJCOSX method.[68, 69]

3. RESULTS AND DISCUSSION

Our results are discussed below in the following manner. We first highlight situations where ωB88PTPSS performs better than one or both of ωB2PLYP and PBE0-2. These cases involve the QR and QCT subsets of the QUESTDB set as well as systems with IST gaps. We then discuss the remaining subsets of QUESTB, where all three DH-DFAs perform fairly well. Lastly, we discuss results obtained for Chl *a* and MR-TADF materials, Scheme 1.

3.1 Doublet-Doublet Excitations: Here we consider performance of several modern DH-DFAs for 42 doublet-doublet excitations of 22 systems, Table 1. These systems were obtained from the QUESTDB #4 dataset.[70] As noted earlier, some of the excitations in this dataset have been classified as QR (radicals) by Liang et al.[53] We compared the DH-DFAs excitation energies against theoretical best estimates (TBEs) previously claimed as being within 0.05 eV of full configuration interaction results after accounting for basis set incompleteness effects. Notice that Van Diyk et al. have previously evaluated the performance of 29 hybrid and DH-DFAs on a similar data set.[71] However, PBE0-2 was not included in this list. Also, we used all excitations selected by Liang et al.[53]

In Table 1, we compare the MAE and RMSEs of ωB2PLYP and PBE0-2 as well as other DH-DFAs for these systems. The MAE of PBE0-2 is comparable to that of M06-2X, a meta-GGA hybrid.[72] The RMSE, which punishes outliers more so than MAE, is even higher for both functionals. By comparison, the

Table 1. Statistical performance of 11 functionals for the QR subset of doublet-doublet excitations. All values are in eV.

	M06-2X	ωB88PTPSS	ωB2PLYP	PBE0-2
MAE	0.38	0.24	0.26	0.43
RMSE	0.50	0.35	0.38	0.56
MAX+	1.54	0.90	1.24	1.74
MAX-	-1.01	-1.07	-1.05	-0.94
	PBE-QIDH	PBE0-DH	ωB88PP86	ωPBEPP86
MAE	0.38	0.30	0.32	0.32
RMSE	0.49	0.39	0.44	0.44
MAX+	1.39	1.39	1.33	1.39
MAX-	-1.02	-1.19	-1.08	-1.00
	SOS-ωB88PP86	SCS/SOS-ωB2PLYP	SCS-ωB2GP-PLYP	
MAE	0.24	0.21	0.22	
RMSE	0.37	0.33	0.36	
MAX+	1.18	1.19	1.30	
MAX-	-1.08	-1.14	-1.08	

MAE for ωB2PLYP is lower by about 0.16 eV, at 0.26 eV. Although, this MAE seems high, we emphasize that the QR dataset also contains a few systems with significant multireference and double-excitation behavior. Indeed, the QR subset considered in this work and by Liang et al.[53] include more difficult excitations than were considered by van Diyk et al.[71] This explains why our MAE for ωB2PLYP (0.26 eV) is significantly higher than theirs, 0.17 eV.

ωB88PTPSS already performs slightly better than ωB2PLYP with an MAE of 0.24 eV. The RMSEs of both functionals are comparable, as are their maximal deviations from the reference values in the positive (overestimation or MAX+) and negative (underestimation or MAX-) directions. Looking back at Liang et al.'s[53] results, the MAE for ωB88PTPSS is already close to the best hybrid meta-GGAs, ωM05-D[73](0.25 eV), BMK[74] (0.23 eV) and PW6B95[75] (0.23 eV). Indeed, Liang et al. obtained the lowest MAE with ωB97X-V, 0.19 eV, a hybrid GGA.[53] Subsequently, we tested other DH-DFAs like SCS/SOS-ωB2PLYP, SOS-ωB88PP86 and SCS-ωB2GP-PLYP on the set of QR doublet-doublet excitations with the same TBEs. These were selected as they had the lowest MAEs in the report by Van Diyk et al.[71] The MAEs of SCS/SOS-ωB2PLYP, SOS-ωB88PP86 and SCS-ωB2GP-PLYP[37] are 0.21, 0.24 and 0.22 eV, respectively, Table 1. These are all within 0.03 eV of ωB88PTPSS, revealing the latter's good performance, without any scaling of SCS/SOS energies. Overall, ωB88PTPSS performs better than PBE0-DH,[7] PBE-QIDH,[8] ωPBEPP86 and ωB88PP86.[37]

3.2 Systems with Inverted Singlet-Triplet Gaps: As noted before, we also considered the same 50 IST systems studied by Alipour and Izadkast.[33] Several of these are shown in Figure 1, while the rest are in the Supporting Information, SI.

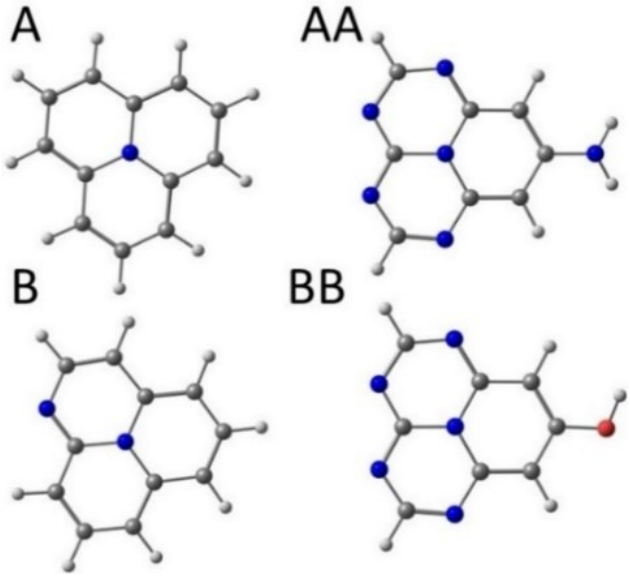

Figure 1. Optimized structures of 4 systems with negative singlet-triplet gaps. Carbon, nitrogen, oxygen, and hydrogen atoms are grey, blue, red, and white spheres, respectively.

S_0-S_1 and S_0-T_1 excitation energies were calculated with TDA-DFT and ΔE_{S1T1} gaps were taken as the differences between the total electronic energies of the S_1 and T_1 states, accounting for the coefficients of E_c^{DFT} and $E_c^{nonlocal}$ in the DH-DFAs.

With ωB88PTPSS, we obtained negative singlet-triplet gaps for all 50 systems, already an improvement on PBE0-2 and dramatically better than ωB2PLYP. The gaps obtained with ωB88PTPSS are compared with reference values in Figure 2. These reference values were obtained with the equation-of-motion coupled-cluster singles and doubles, EOM-CCSD, method.[76] Some caution with using EOM-CCSD as a reference is required as workers have previously reported differences between the negative energy gaps predicted by EOM-CCSD and other wavefunction methods.[34, 77-79] The maximum deviations of ωB88PTPSS from EOM-CCSD were obtained for **A**, **B**, **NN**, **PP**, **RR**, **SS**, **TT**, **UU**, **VV**, **WW** and **XX**, with deviations of 0.04-0.16 eV. For many of these, ωB88PTPSS predicts even larger negative gaps than the EOM-CCSD reference. For the remaining 39 systems, ωB88PTPSS provides energy gaps within 0.04 eV of the EOM-CCSD reference. The most worrisome system for ωB88PTPSS is **B**, for which we got a small but still negative IST gap of -0.002 eV. ωB88PTPSS has an MAD of 0.04 eV, an MSD of 0.01 eV and an RMSD of 0.06 eV. This is compared to the

best performing SOS0-CIS(D)-PBE-QIDH functional with MSD, MAD and RMSD of -0.02, 0.02 and 0.03 eV, respectively, indicating that ωB88PTPSS is competitive with all DH-DFAs studied previously, without scaling non-local correlation energies.[33]

Figure 2. Inverted singlet-triplet gaps of 50 systems provided by TDA-DFT calculations with ωB88PTPSS are compared with EOM-CCSD and SOS-PBE-QIDH data.

To highlight the good progress of ωB88PTPSS, we note that SCS/SOS-ωB2PLYP, the SCS/SOS variant of ωB2PLYP yields positive energy gaps for 29 out of 50 systems. SCS-ωB2GP-PLYP gives positive energy gaps for 4 systems while ωP-BEPP86 and SCS-ωB88PP86 yield positive energy gaps for 7 systems. SOS-ωB88PP86 yields 2 positive gaps. SOS-ωB2GP-PLYP has MSD, MAE and RMSE of 0.03, 0.03 and 0.04 eV, respectively. This is close to ωB88PTPSS, however, it yields a vanishingly small but positive gap for **HH**. Moreover, the SOS-variant of ωPBEPP86, SOS-ωPBEPP86, yields negative IST gaps for all 50 systems, but has slightly worse MSD, MAD and RMSD values of -0.07, 0.07 and 0.08 eV, relative to the reference.[33] For us, ωB88PTPSS is very promising due to its similar performance for doublet-doublet excitations, Table 1, its ability to capture negative singlet-triplet gaps for 50 IST systems, Figure 2, and its statistical performance compared to the EOM-CCSD reference for IST gaps.

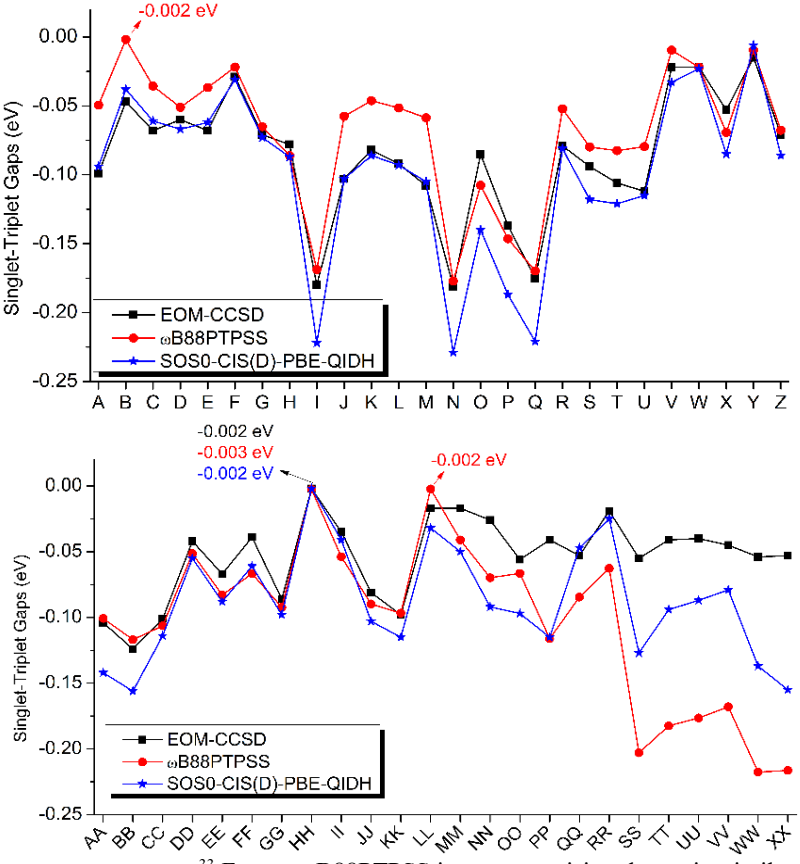

We can comment on ωB88PTPSS's good performance in light of a report by Ghosh and Bhattacharyya.[80] They considered 7 systems, most of which are among the species studied in this work. They concluded that successful prediction of IST gaps requires more than 45% nonlocal contribution to the correlation energy as well as more than 50% contribution of exact exchange to the exchange energy. Observe that Sancho-Garcia et al. also reported that a minimum of 50% MP2 correlation is needed to obtain negative gaps.[35] ωB88PTPSS conforms to these requirements. Ghosh and Bhattacharyya found the DH-DFA ωB97X-2 predicts negative energy gaps for all 7 systems.[81] It however massively overestimates IST gaps for all systems.[80]

3.3 Intra-molecular Charge-Transfer Excitations: Liang et al. created a QCT subset focused on charge-transfer (CT) excitations from the QUESTDB #6 set.[53] They omitted the dipeptide and β-peptide from QUESTDB #6 and found that the best performing DFAs are CAM-B3LYP[82] and LRC-ωPBEh[83] with MAEs of 0.18 and 0.19 eV, respectively. The RMSEs of these functionals were 0.23 and 0.24 eV, respectively. Mester and Kallay have also studied these systems, including dipeptide and β-peptide in their list.[84] Notice however that they used TBEs obtained at the cc-pVTZ level as their reference data. However, Liang et al. used TBEs obtained with aug-cc-pVTZ basis sets.[53] The aug-cc-pVTZ TBEs are always within 0.02 eV of aug-cc-pVQZ TBEs.[85] By contrast, cc-pVTZ TBEs deviate from aug-cc-pVQZ TBEs by 0.02-0.39 eV, with an average deviation of 0.12 eV. Considering this, we chose to use the aug-cc-pVTZ TBEs like Liang et al.[53] and omit the dipeptide and β-peptide. Thus, we analyzed 27 CT excitations in 17 different systems.

Moreover, evaluating the performance of DH-DFAs for the QCT subset is important since CT states are often crucial to rigorous descriptions of molecular conductance and electron transfer behavior. This is because CT states correspond to the presence of the particle and hole densities on separate parts of a molecule or supermolecule.[86, 87] Notice however that the QCT subset pertains only to intramolecular excitations. However, range-separated hybrids, like CAM-B3LYP and LRC-ωPBEh, can provide fairly good descriptions of such excitations.[88-91] Notice also that Liang et al.[53] found that PBE0 has an MAE of 0.41 eV, compared to 0.32 eV for PBE50 and 0.28 eV for BHHLYP.[92] This conforms to literature experience indicating that CT states are better described with DFAs with large amounts of exact exchange. We thus compare the performance of ωB88PTPSS to CAM-B3LYP and LRC-ωPBEh. Crucially also, we focus on comparing ωB88PTPSS to the two DFAs that motivated our work, ωB2PLYP and PBE0-2. Our calculations were performed in a similar manner as for the QR subset, see SI.

SOS-ωB88PP86 and SCS-ωB2GP-PLYP performed quite well, with MAEs of 0.17 eV. This is slightly better than the MAEs of CAM-B3LYP and LRC-ωPBEh, Table 2. This is not surprising since SOS-ωB88PP86 and SCS-ωB2GP-PLYP were found to be top performers in the report by Mester and Kallay.[84] Remarkably, the MAEs of SOS-ωB88PP86 and SCS-ωB2GP-PLYP are a full 0.10 eV better than for ωB2PLYP. On the other hand, SCS/SOS-ωB2PLYP gave a 0.04 eV improvement on ωB2PLYP. SOS-ωB88PP86 also improved on ωB88PP86 by about 0.05 eV. In this situation, the SCS and SOS variants are clearly beneficial.[19, 37, 84] Notice however that Table 2 shows that ωB88PTPSS has a MAE of 0.18 eV, comparable with CAM-B3LYP, LRC-ωPBEh, SOS-ωB88PP86 and SCS-ωB2GP-PLYP; a bit better than PBE0-2 and much improved over ωB2PLYP. The RMSE of ωB88PTPSS is also the smallest of all these functionals, although its error interval (range of MAX+ to MAX-) is larger than for CAM-B3LYP and LRC-ωPBEh.

Table 2. Performance of 11 functionals for the QCT subset. All values are in eV and were obtained with aug-cc-pVTZ.

	M06-2X	ωB88PTPSS	ωB2PLYP	PBE0-2
MAE	0.24	0.18	0.28	0.23
RMSE	0.31	0.22	0.33	0.29
MAX+	0.57	0.44	0.65	0.95

MAX-	-0.70	-0.49	-0.06	-0.16
	PBE-QIDH	PBE0-DH	ωB88PP86	ωPBEPP86
MAE	0.21	0.20	0.22	0.25
RMSE	0.28	0.28	0.29	0.32
MAX+	0.95	0.86	1.01	1.13
MAX-	-0.14	-0.36	-0.20	-0.23
	SOS-ωB88PP86	SCS/SOS-ωB2PLYP	SCS-ωB2GP-PLYP	
MAE	0.17	0.23	0.17	
RMSE	0.26	0.29	0.25	
MAX+	1.00	0.97	0.89	
MAX-	-0.45	-0.33	-0.39	

3.4 Other Subsets from QUESTDB: Thus far, we showed that ωB88PTPSS performs better than ωB2PLYP and PBE0-2 for IST systems and provides excellent agreement with TBEs for intramolecular CT excitations. We now consider the rest of the QUESTDB database, for which both ωB2PLYP and PBE0-2 perform fairly well.[38] Excitations from the other subsets of QUESTDB were classified as QE[70] (exotics), Q2 and Q1 by Liang et al.[53] The systems in the Q2 subset have up to 10 non-hydrogen atoms while those in Q1 have a maximum of 4 non-hydrogen atoms.

For the QE subset, Liang et al. found the best performance with M06-SX, ωB97X-D and BMK, with MAEs of about 0.20 eV, spanning singlet-singlet and singlet-triplet excitations.[53] This is quite good, especially when considering that second-order algebraic diagrammatic construction, [ADC(2)][93] and second-order approximate coupled cluster (CC2)[94] have MAEs of 0.15 and 0.12 eV, respectively. For the singlet-singlet excitations, ωB2PLYP has a MAE of 0.13 eV while for the singlet-triplet excitations, it has an MAE of 0.21 eV, for a total MAE of 0.16 eV, indicating that ωB2PLYP has near-CC2-quality for these species, Table 3. The MAE for singlet-singlet excitations is close to the one obtained by on the Loos and Jacquemin benchmark of 11 molecules out of 14 in the QE subset, 0.15 eV.[37] Remarkably, PBE0-2 does even better, MAE of 0.11 eV for singlet excitations and 0.11 eV for excitation to triplet states, for a total of MAE of 0.11 eV. ωB88PTPSS has an MAE of 0.11 eV for singlet-singlet excitations and an MAE of 0.20 eV for excitations to triplet states, giving a total MAE of 0.14 eV. We therefore conclude that ωB88PTPSS, like PBE0-2 and ωB2PLYP, has near-ADC(2) accuracy for the QE subset. This conclusion extends to all other DH-DFAs that we tested, which all perform better than LDAs, GGAs, hybrid GGAs, meta GGAs and hybrid meta-GGAs tested previously.[53] Overall, for the QE subset, ωB88PTPSS *did* not degrade the already excellent performances of PBE0-2 and ωB2PLYP.

Table 3. Performance of 11 functionals for the QE subset. All values are in eV and were obtained with aug-cc-pVTZ.

	M06-2X	ωB88PTPSS	ωB2PLYP	PBE0-2
MAE	0.26	0.14	0.16	0.11
RMSE	0.29	0.18	0.19	0.15
MAX+	0.25	0.23	0.22	0.33
MAX-	-0.89	-0.41	-0.39	-0.31
	PBE-QIDH	PBE0-DH	ωB88PP86	ωPBEPP86
MAE	0.15	0.17	0.13	0.12
RMSE	0.18	0.22	0.16	0.15
MAX+	0.43	0.27	0.43	0.34
MAX-	-0.35	-0.45	-0.3	-0.27
	SOS-ωB88PP86	SCS/SOS-ωB2PLYP	SCS-ωB2GP-PLYP	
MAE	0.14	0.13	0.12	
RMSE	0.17	0.16	0.15	
MAX+	0.51	0.22	0.40	
MAX-	-0.27	-0.35	-0.26	

The Q1 and Q2 subsets of QUESTDB are so large that we restricted ourselves to a simpler issue, examining the performance of only ωB88PTPSS and ωB2PLYP. We found that both DH-DFAs achieve accuracies of near-CC2 and near-ADC(2) quality. In Figure 3, we provide the statistical performance for both functionals. Observe that for Figure 3, the vertical axis starts from -0.1 eV in order to accommodate the MSEs for both DFAs, ADC(2) and CC2. For instance, the MSEs of ωB2PLYP and ωB88PTPSS are -0.07 and -0.08 eV, respectively for the Q1 set. For the Q2 set, their MSEs are 0.11 and 0.02 eV, respectively.

For Q1 and Q2, ωB88PTPSS has overall MAEs of 0.21 and 0.16 eV, respectively. These are comparable to CC2 MAEs of 0.22 and 0.14 eV, respectively, and ADC(2), 0.21 and 0.13 eV,

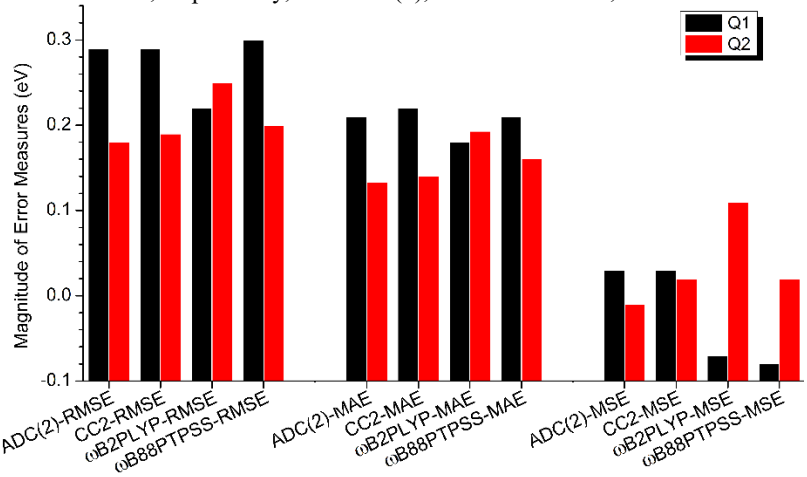

Figure 3. Performance of ωB88PTPSS and ωB2PLYP for Q1 and Q2 subsets of QUESTDB. Statistics for CC2 and ADC(2) are taken from reference [53].

respectively. ADC(2) and CC2 data are taken from the SI of reference [53]. ωB2PLYP remains quite a formidable DH-DFA, with MAEs of 0.18 and 0.19 eV, for Q1 and Q2, respectively. Mester and Kallay previously obtained an MAE of 0.17 eV for the Q1 database with ωB2PLYP.[84] Looking back, Liang et al., found that the best hybrid GGAs and hybrid meta-GGAs all have MAEs of around 0.20 eV for the Q1 subset, and are therefore competitive with ωB2PLYP, ωB88PTPSS, CC2 and ADC(2).[53] Specifically M06-SX,[95] BMK,[74] ωB97X-V[96] and SOGGA11-X[97] have MAEs of 0.20, 0.21, 0.20 and 0.21 eV, respectively for the Q1 set.

For the Q2 dataset of organic species, the best performing hybrid GGA is ωB97X with a MAE of 0.18 eV. All other functionals tested by Liang et al. had MAEs exceeding 0.20 eV.[53] Therefore, the hybrid GGAs and meta-GGAs are not as accurate as ωB2PLYP, ωB88PTPSS, CC2 and ADC(2). The RMSEs and MSEs of ωB88PTPSS, CC2 and ADC(2) are better than all DFAs tested by Liang et al.[53]

3.5 Other Examples from the Literature: Having seen the performance of ωB88PTPSS for all electronic absorptions in the entire QUESTDB set, we now consider two "*real-life*" examples from the very recent literature. Specifically, we consider large systems of importance in photochemistry and materials design. Prior to that, we seek to emphasize that the overall MAEs for the Q1, Q2, QE, QR and QCT subsets are 0.20 and 0.18 eV for ωB2PLYP and ωB88PTPSS, respectively. The difference between these MAE values is very small, primarily because the

QUESTDB set is heavily dominated by the large Q1 and Q2 subsets, where ωB2PLYP is particularly strong. Interestingly, the training set for ωB2PLYP contained several systems found in Q1 and Q2.[27] Nevertheless, we have seen keen differences in the behaviors of ωB2PLYP and ωB88PTPSS for the QCT subset and for IST systems. For perspective, King et al. have reported MAEs of 0.18, 0.19, 0.42, 0.15, and 0.15 eV for NEVPT2,[98] tPBE0,[99] SA-CASSCF, ADC(2) and CC2 over 373 excitations.[100]

In the first "*real-life*" example, we consider low-energy excited states in the Q and B bands of chlorophyll *a*, (Chl *a*) studied recently by Sirohiwal et al.[54] with DLPNO-STEOM-CCSD[101-103] and TD-DFT methods. Notice that they used full TD-DFT, not TDA-DFT. DLPNO-STEOM-CCSD agrees quite well with quasi-experimental vertical excitation energies, Table 4. They obtained Q_y, Q_x, B_x and B_y bands of 1.75, 2.24, 3.17 and 3.40 eV at the CAM-B3LYP-optimized geometry. These are to be compared against quasi-experimental values (QEVs) at 1.99, 2.30, 3.12 and 3.38 eV, respectively.

Table 4. Vertical excitation energies (eV) of Chl *a* at the CAM-B3LYP gas-phase geometry. DLPNO-STEOM-CCSD is depicted as DLPNO-STEOM. Quasi-experimental values (QEVs) and B2PLYP data are taken from reference [54]. Gaps between the B_y and lowest N transitions are also given.

Method	Q_y	Q_x	B_x	B_y	Gap	MAD(MSD)
DLPNO-STEOM	1.75	2.24	3.17	3.40	0.114	0.10 (-0.07)
B2PLYP	2.12	2.23	3.17	3.27	0.003	0.09 (+0.00)
ωB2PLYP	2.04	2.49	3.45	3.78	0.045	0.24 (+0.24)
SCS/SOS-ωB2PLYP	1.81	2.35	3.35	3.68	0.061	0.19 (+0.10)
ωB2GP-PLYP	2.04	2.41	3.42	3.74	0.083	0.20 (+0.20)
SCS-ωB2GP-PLYP	1.69	2.12	3.22	3.53	0.104	0.18 (-0.06)
ωB88PP86	2.07	2.28	3.33	3.57	0.097	0.12 (+0.11)
ωPBEPP86	2.07	2.22	3.30	3.52	0.091	0.12 (+0.08)
SCS-ωPBEPP86	1.65	1.90	3.11	3.34	0.074	0.20 (-0.20)
SOS-ωPBEPP86	1.67	2.04	3.18	3.43	0.059	0.17 (-0.12)
PBE0-2	2.10	2.17	3.27	3.48	0.090	0.12 (+0.06)
PBE-QIDH	2.12	2.30	3.32	3.52	0.079	0.12 (+0.12)
ωB88PTPSS	2.02	2.16	3.26	3.47	0.104	0.10 (+0.03)
QEV	1.99	2.30	3.12	3.38		

Also, DLPNO-STEOM-CCSD describes the low-energy bands of Chl *a* in a way that conforms quite well to the four-orbital Gouterman model.[104, 105] By contrast, TD-DFT without MP2 corrections (*non*-DH DFAs) predicted excitations that do not conform to the Gouterman model, i.e. ghost states with low oscillator strengths between the Q_x and B_x or between the B bands. DH-DFAs like B2PLYP and ωB2PLYP provided the same ordering of excited states as DLPNO-STEOM-CCSD, but with the first N transitions being essentially isoenergetic with the B_y band. Also, notice in Table 4 that ωB2PLYP severely overestimates the energies of the B_x and B_y bands. Details of our calculations are provided in the SI. Results of 10 DH-DFAs are given in Table 4. Results for 23 other DH-DFAs are in the SI.

ωB88PTPSS ameliorates overestimation of the B bands by ωB2PLYP, Table 4. Analysis of the excitations shows that their characters match exactly with DLPNO-STEOM-CCSD. For example, the B_y band is dominated by the HOMO-1 → LUMO+1 and HOMO → LUMO transitions, just as in DLPNO-STEOM-CCSD, see SI for details. Compared against the QEVs, we see that ωB88PTPSS has a MAD of 0.10 eV and an MSD of 0.03 eV. This is very close to the statistical performance of DLPNO-STEOM-CCSD, MAD of 0.10 eV and MSD of -0.07 eV. Compared to ωB2PLYP, we see that the statistical performance of ωB88PTPSS is much better. Also, ωB88PTPSS does slightly better than PBE0-2. In Table 4, the best statistical performance is from B2PLYP, with an MAD of 0.09 eV and an MSD of 0.00 eV. However, B2PLYP separates the B_y band from the lowest N transitions by only 0.003 eV. This was previously pointed out by Sirohiwal et al. as a crucial error for this DH-DFA.[54] In the SI, there are 7 other DH-DFAs that have MADs around 0.07-0.10 eV. Like B2PLYP, they all have too small gaps between the B_y band and lowest N transitions. The gap to N transitions is 0.114 eV from DLPNO-STEOM-CCSD. For ωB2PLYP, the gap to these transitions is 0.045 eV while for ωB88PTPSS, the gap is 0.104 eV. The newer ωB88PP86 and ωPBEPP86 perform much better than ωB2PLYP, statistically as well as in predictions of B_y-to-N gaps, Table 4. Compared to these two DH-DFAs, ωB88PTPSS has better statistical performance. The B_y-to-N gap is also slightly wider with ωB88PTPSS. We also surprisingly find that the SCS and SOS variants are in many cases less accurate than their original DFAs. This is interesting as SCS and SOS variants generally improved the statistical performance when used on the QUESTDB database containing 10 or less non-hydrogen atoms. However, for a '*real-life*' example like Chl *a*, they often make things just quite worse, partly justifying the current work, see SI for details. Only ωB88PTPSS, out of 33 tested DH-DFAs, simultaneously achieves an MAD ≤ 0.10 and a B_y-to-N gap ≥ 0.10 eV. Thus, ωB88PTPSS provides an accurate qualitative and quantitative description of the low energy bands of Chl *a*.

In the second example, we consider three MR-TADF chromophores examined recently by Hall et al.[55] These systems are OQAO, SQAO and DIKTA, Figure 4. We refer the reader to reference [106-110] for description of TADF and MR-TADF systems. Hall studied MR-TADF systems with TDA-DFT, TD-DFT and SCS-CC2, calculating excitation energies to the lowest singlet (S_1) and triplet (T_1) states, as well as the gaps between these two states, ΔE_{S1T1}.[55] Calculated $S_0 \rightarrow S_1$ and $S_0 \rightarrow T_1$ excitation energies of these systems are best compared to SCS-CC2 data

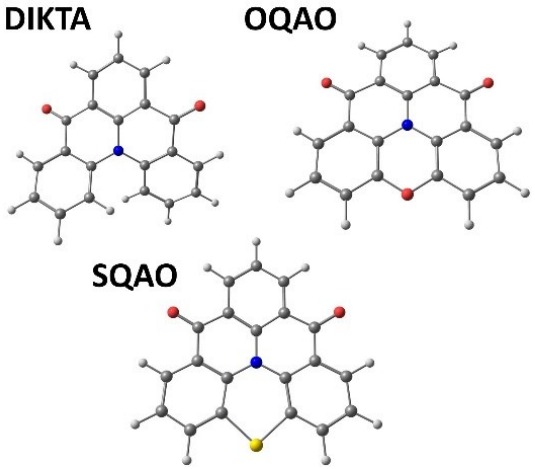

Figure 4. Structures of 3 MR-TADF materials. Carbon, nitrogen, oxygen, and hydrogen atoms are grey, blue, red, and white spheres, respectively.

as experimental measurements were performed in condensed media. ΔE_{S1T1} gaps can however be compared to experimental data as well as SCS-CC2 results.

The performance of the 10 DH-DFTs are presented in Table 5. Excitation energies from SOS-ωPBEPP86 are very close to SCS-CC2, MAD of 0.005 eV for excitations to S_1 and 0.034 eV to the T_1 state. ωB88PTPSS and B2PLYP, are the next closest to SCS-CC2. ωPBEPP86 and SCS-ωPBEPP86 also cluster well around SCS-CC2. However, as seen for Chl *a* in Table 4, we see that ωB2PLYP and ωBGP-PLYP dramatically overestimate the excitation energies to the lowest singlet states, while doing much better for triplet states. For PBE0-2, the triplet excitation energies have greater deviations from SCS-CC2. This imbalance means that PBE0-2, ωB2PLYP and ωBGP-PLY DFAs have MADs of 0.098, 0.424 and 0.293 eV, respectively for the ΔE_{S1T1} gaps. The SCS and SOS variants of these functionals provide some improvement, but their MADs for singlet-triplet ΔE_{S1T1} gaps still mostly exceed 0.07 eV. ωB88PTPSS has an MAD of 0.052 eV for ΔE_{S1T1} gaps, although SOS-ωPBEPP86, ωP-BEPP86 and B2P-PLYP also do well. Our data therefore reveals that the $S_0 \rightarrow S_1$ and $S_0 \rightarrow T_1$

Table 5. Performance of 10 DH-DFAs and SCS-CC2 for excitation energies and ΔE_{S1T1} gaps of 3 MR-TADF systems. Excitation energies are compared to SCS-CC2 data while ΔE_{S1T1} gaps are compared to experimental data from reference [55]. MADs are given in eV while MSDs are in parenthesis.

Method	$S_0 \rightarrow S_1$	$S_0 \rightarrow T_1$	ΔE_{S1T1}
B2PLYP	0.035 (-0.022)	0.035 (-0.051)	0.049 (0.049)
ωB2PLYP	0.426 (0.426)	0.059 (0.059)	0.424 (0.424)
SCS/SOS-ωB2PLYP	0.296 (0.296)	0.037 (0.037)	0.315 (0.315)
ωB2GP-PLYP	0.377 (0.377)	0.141 (0.141)	0.293 (0.293)
SCS-ωB2GP-PLYP	0.154 (0.154)	0.048 (0.048)	0.163 (0.163)
SOS-ωB2GP-PLYP	0.205 (0.205)	0.104 (0.104)	0.157 (0.157)
ωPBEPP86	0.074 (0.074)	0.074 (0.074)	0.057 (0.057)
SCS-ωPBEPP86	0.082 (-0.082)	0.107 (-0.107)	0.082 (0.082)
SOS-ωPBEPP86	0.005 (-0.004)	0.034 (-0.002)	0.054 (0.054)
PBE0-2	0.045 (0.045)	0.182 (0.182)	0.098 (-0.080)
PBE-QIDH	0.064 (0.064)	0.083 (-0.083)	0.203 (0.203)
ωB88PTPSS	0.013 (-0.010)	0.032 (0.015)	0.052 (0.052)
SCS-CC2	0.000 (0.000)	0.000 (0.000)	0.057 (0.057)

excitation energies as well as ΔE_{S1T1}gaps are not problematic for these 4 DH-DFAs. Indeed, Table 5 shows that using DH-DFAs can provide agreement with wavefunction theory-based (WFT) methods as well as experimental data. Rather, the major problem for all tested DH-DFAs are intermediate ghost and dark singlet states with low oscillator strengths near S_1 (as mostly S_2 and S_3), especially in the case of SQAO and OQAO. These ghost states are absent in SCS-CC2 and other WFT calculations, and likely complicate spin-vibronic descriptions of the TADF and MR-TADF phenomena.[55]

4. CONCLUSIONS

To explore the possibility of using a double-hybrid density functional approximation (DH-DFA) for simultaneous and accurate description of excitation energies as well as non-conventional systems with inverted singlet-triplet (IST) gaps, we modified the popular ωB2PLYP exchange-correlation density functional. The new functional is ωB88PTPSS, and it utilizes equipartition (50%:50%) of the correlation energy between the semilocal DFT and nonlocal wavefunction parts; while employing the TPSS meta-GGA correlation functional. As ωB88PTPSS is developed and validated only for excitation energies, we have compared the performance of ωB2PLYP and ωB88PTPSS, as well as modern DH-DFAs that employ same-spin, SCS, and opposite-spin, SOS, scaling of the nonlocal correlation energy. We tested these functionals on previously selected Q1, Q2, QR, QE and QCT subsets of excitations from the QUESTDB database. We also investigated the performance of these methods for a set of 50 IST systems as well as several systems of interest in photochemistry and materials design, chlorophyll *a* and a set of multi-resonant thermally active delayed fluorescence, TADF, organic emitters.

We find ωB88PTPSS loses no ground in terms of accuracy and to our satisfaction, it performs almost as well or better than some of the latest DH-DFAs that utilize SS and OS scaling of MP2 and CIS(D) correlation energies, in nearly all cases. We showed that for excitations in open-shell systems (QR subset), ωB88PTPSS performs as well as modern DH-DFAs. For the Q3E subset, ωB88PTPSS achieves CC2 and ADC(2) quality. Crucially, ωB2PLYP and ωB88PTPSS both achieve CC2 and ADC(2) quality for the Q1 and Q2 subsets; while for intramolecular CT excitations, ωB88PTPSS performs much better than ωB2PLYP and is competitive with modern SCS/SOS DH-DFAs. For non-conventional systems with inverted singlet-triplet (IST) gaps, ωB88PTPSS is clearly superior to ωB2PLYP, correctly delivering negative gaps, even when many SCS/SOS DH-DFAs fail. Compared to EOM-CCSD reference data for negative gaps of IST systems, ωB88PTPSS has an MAD of only 0.04 eV. Subsequently, we examined the performance of ωB88PTPSS for several large systems. For chlorophyll *a*, ωB88PTPSS is the only DH-DFA, out of 33 tested, that simultaneously delivers a MAD $\leq$ 0.10 eV as well as a B_y-to-N gap $\geq$ 0.10 eV, exactly like DLPNO-STEOM-CCSD. Surprisingly for chlorophyll *a*, the SCS/SOS DFAs are mostly detrimental. Lastly, for a small set of TADF systems, ωB88PTPSS provides excellent agreement with SCS-CC2 excitation energies and does remarkably well for the gaps between S_1 and T_1 states. Going forward, ωB88PTPSS could be improved for excitation energies by reworking the range-separated exchange with a SR meta-GGA exchange functional.[111]

SUPPLEMENTARY MATERIAL

See the supplementary material for our TD-DFT and TDA-DFT procedures, raw excitation energies and analysis procedures,

Cartesian coordinates of Chlorophyll-*a* and MR-TADF materials.

ACKNOWLEDGMENT

S.O.O thanks the NSF (1800387) for generous funding. We also acknowledge Yoann Olivier of the University of Namur for providing us SCS-CC2-optimized geometries of MR-TADF emitters.

DATA AVAILABILITY

The data that supports the findings of this study are available within the article and its supplementary material.

REFERENCES

1. K. Burke, J. Werschnik and E. K. U. Gross, Journal of Chemical Physics **123** (2005).
2. A. Dreuw and M. Head-Gordon, Chemical Reviews **105**, 4009-4037 (2005).
3. M. A. L. Marques and E. K. U. Gross, Annual Review of Physical Chemistry **55**, 427-455 (2004).
4. E. Runge and E. K. U. Gross, Physical Review Letters **52**, 997-1000 (1984).
5. in *Recent Advances in Computational Chemistry* (WORLD SCIENTIFIC, 1995), Vol. Volume 1, pp. 428.
6. M. Veril, A. Scemama, M. Caffarel, F. Lipparini, M. Boggio-Pasqua, D. Jacquemin and P. F. Loos, Wiley Interdisciplinary Reviews-Computational Molecular Science **11**, e1517 (2021).
7. E. Bremond and C. Adamo, Journal of Chemical Physics **135** (2011).
8. E. Bremond, J. C. Sancho-Garcia, A. J. Perez-Jimenez and C. Adamo, Journal of Chemical Physics **141** (2014).
9. L. Goerigk and S. Grimme, J. Chem. Theory Comput. **7**, 3272-3277 (2011).
10. K. Sharkas, J. Toulouse and A. Savin, Journal of Chemical Physics **134** (2011).
11. M. Feyereisen, G. Fitzgerald and A. Komornicki, Chemical Physics Letters **208**, 359-363 (1993).
12. M. Headgordon, J. A. Pople and M. J. Frisch, Chemical Physics Letters **153**, 503-506 (1988).
13. C. Møller and M. S. Plesset, Physical Review **46**, 618-622 (1934).
14. S. Grimme, Journal of Chemical Physics **124**, 034108 (2006).
15. Y. Zhao, B. J. Lynch and D. G. Truhlar, Journal of Physical Chemistry A **108**, 4786-4791 (2004).
16. M. Head-Gordon, R. J. Rico, M. Oumi and T. J. Lee, Chemical Physics Letters **219**, 21-29 (1994).
17. S. Grimme and F. Neese, The Journal of Chemical Physics **127**, 154116 (2007).
18. M. Casanova-Paez and L. Goerigk, Journal of Chemical Physics **153** (2020).
19. M. Casanova-Paez and L. Goerigk, Journal of Computational Chemistry **42**, 528-533 (2021).
20. L. Goerigk and S. Grimme, Wiley Interdisciplinary Reviews-Computational Molecular Science **4**, 576-600 (2014).
21. N. Mehta, M. Casanova-Paez and L. Goerigk, Physical Chemistry Chemical Physics **20**, 23175-23194 (2018).
22. A. Najibi, M. Casanova-Paez and L. Goerigk, Journal of Physical Chemistry A **125**, 4026-4035 (2021).
23. R. Baer and D. Neuhauser, Physical Review Letters **94** (2005).
24. H. Iikura, T. Tsuneda, T. Yanai and K. Hirao, Journal of Chemical Physics **115**, 3540-3544 (2001).
25. C. Kalai and J. Toulouse, Journal of Chemical Physics **148** (2018).
26. T. Tsuneda and K. Hirao, Wiley Interdisciplinary Reviews-Computational Molecular Science **4**, 375-390 (2014).
27. M. Casanova-Páez, M. B. Dardis and L. Goerigk, J. Chem. Theory Comput. **15**, 4735-4744 (2019).
28. O. Adeyiga, O. Suleiman and S. O. Odoh, Inorganic Chemistry **60**, 8489-8499 (2021).
29. K. Curtis, D. Panthi and S. O. Odoh, Inorganic Chemistry **60**, 1150-1160 (2021).
30. O. Suleiman, D. Panthi, O. Adeyiga and S. O. Odoh, Inorganic Chemistry **60**, 6218-6227 (2021).
31. A. D. Becke, Physical Review A **38**, 3098-3100 (1988).
32. C. Lee, W. Yang and R. G. Parr, Physical Review B **37**, 785-789 (1988).
33. M. Alipour and T. Izadkhast, The Journal of Chemical Physics **156**, 064302 (2022).
34. J. Sanz-Rodrigo, G. Ricci, Y. Olivier and J. C. Sancho-Garcia, Journal of Physical Chemistry A **125**, 513-522 (2021).
35. J. C. Sancho-García, E. Brémond, G. Ricci, A. J. Pérez-Jiménez, Y. Olivier and C.

Adamo, The Journal of Chemical Physics **156**, 034105 (2022).
36. J.-D. Chai and S.-P. Mao, Chemical Physics Letters **538**, 121-125 (2012).
37. M. Casanova-Páez and L. Goerigk, J. Chem. Theory Comput. **17**, 5165-5186 (2021).
38. D. Mester and M. Kállay, J. Chem. Theory Comput. **17**, 927-942 (2021).
39. M. Alipour and N. Karimi, J. Chem. Theory Comput. **17**, 4077-4091 (2021).
40. R. Peverati and D. G. Truhlar, The Journal of Physical Chemistry Letters **2**, 2810-2817 (2011).
41. J. Tao, J. P. Perdew, V. N. Staroverov and G. E. Scuseria, Physical Review Letters **91**, 146401 (2003).
42. J. P. Perdew, A. Ruzsinszky, J. Tao, V. N. Staroverov, G. E. Scuseria and G. I. Csonka, The Journal of Chemical Physics **123**, 062201 (2005).
43. M. Alipour, Chemical Physics Letters **623**, 14-16 (2015).
44. J. Sun, A. Ruzsinszky and J. P. Perdew, Physical Review Letters **115**, 036402 (2015).
45. G. Santra, N. Sylvetsky and J. M. L. Martin, The Journal of Physical Chemistry A **123**, 5129-5143 (2019).
46. S. M. O. Souvi, K. Sharkas and J. Toulouse, The Journal of Chemical Physics **140**, 084107 (2014).
47. L. Goerigk and S. Grimme, J. Chem. Theory Comput. **7**, 291-309 (2011).
48. S. Kozuch and J. M. L. Martin, Journal of Computational Chemistry **34**, 2327-2344 (2013).
49. Y. Zhang, X. Xu and W. A. Goddard, Proceedings of the National Academy of Sciences of the United States of America **106**, 4963-4968 (2009).
50. N. Mardirossian and M. Head-Gordon, The Journal of Chemical Physics **148**, 241736 (2018).
51. K. Hui and J.-D. Chai, The Journal of Chemical Physics **144**, 044114 (2016).
52. É. Brémond, A. Ottochian, Á. J. Pérez-Jiménez, I. Ciofini, G. Scalmani, M. J. Frisch, J. C. Sancho-García and C. Adamo, Journal of Computational Chemistry **42**, 970-981 (2021).
53. J. Liang, X. Feng, D. Hait and M. Head-Gordon, J. Chem. Theory Comput. **18**, 3460-3473 (2022).
54. A. Sirohiwal, R. Berraud-Pache, F. Neese, R. Izsák and D. A. Pantazis, The Journal of Physical Chemistry B **124**, 8761-8771 (2020).
55. D. Hall, J. C. Sancho-García, A. Pershin, G. Ricci, D. Beljonne, E. Zysman-Colman and Y. Olivier, J. Chem. Theory Comput. **18**, 4903-4918 (2022).
56. T. H. Dunning, Journal of Chemical Physics **90**, 1007-1023 (1989).
57. R. A. Kendall, T. H. Dunning and R. J. Harrison, Journal of Chemical Physics **96**, 6796-6806 (1992).
58. D. E. Woon and T. H. Dunning, Journal of Chemical Physics **98**, 1358-1371 (1993).
59. F. Weigend and R. Ahlrichs, Physical Chemistry Chemical Physics **7**, 3297-3305 (2005).
60. A. D. Becke, J. Chem. Phys. **98**, 5648-5652 (1993).
61. A. D. Becke and E. R. Johnson, Journal of Chemical Physics **123**, 154101 (2005).
62. A. D. Becke and E. R. Johnson, Journal of Chemical Physics **124**, 014104 (2006).
63. S. Grimme, J. Antony, S. Ehrlich and H. Krieg, Journal of Chemical Physics **132**, 154104 (2010).
64. S. Grimme, S. Ehrlich and L. Goerigk, Journal of Computational Chemistry **32**, 1456-1465 (2011).
65. E. Epifanovsky, et al., The Journal of Chemical Physics **155**, 084801 (2021).
66. F. Neese, Wiley Interdisciplinary Reviews-Computational Molecular Science **12**, e1606 (2022).
67. F. Neese, F. Wennmohs, U. Becker and C. Riplinger, Journal of Chemical Physics **152**, 224108 (2020).
68. B. Helmich-Paris, B. de Souza, F. Neese and R. Izsak, Journal of Chemical Physics **155** (2021).
69. R. Izsak and F. Neese, Journal of Chemical Physics **135** (2011).
70. P.-F. Loos, A. Scemama, M. Boggio-Pasqua and D. Jacquemin, J. Chem. Theory Comput. **16**, 3720-3736 (2020).
71. J. Van Dijk, M. Casanova-Páez and L. Goerigk, ACS Physical Chemistry Au **2**, 407-416 (2022).
72. Y. Zhao and D. G. Truhlar, Theoretical Chemistry Accounts **120**, 215-241 (2008).

73. Y.-S. Lin, C.-W. Tsai, G.-D. Li and J.-D. Chai, The Journal of Chemical Physics **136**, 154109 (2012).
74. A. D. Boese and J. M. L. Martin, The Journal of Chemical Physics **121**, 3405-3416 (2004).
75. Y. Zhao and D. G. Truhlar, The Journal of Physical Chemistry A **109**, 5656-5667 (2005).
76. J. Geertsen, M. Rittby and R. J. Bartlett, Chemical Physics Letters **164**, 57-62 (1989).
77. P. de Silva, Journal of Physical Chemistry Letters **10**, 5674-5679 (2019).
78. R. Pollice, P. Friederich, C. Lavigne, G. D. Gomes and A. Aspuru-Guzik, Matter **4**, 1654-1682 (2021).
79. G. Ricci, E. San-Fabian, Y. Olivier and J. C. Sancho-Garcia, Chemphyschem **22**, 553-560 (2021).
80. S. Ghosh and K. Bhattacharyya, The Journal of Physical Chemistry A **126**, 1378-1385 (2022).
81. J.-D. Chai and M. Head-Gordon, The Journal of Chemical Physics **131**, 174105 (2009).
82. T. Yanai, D. P. Tew and N. C. Handy, Chemical Physics Letters **393**, 51-57 (2004).
83. M. A. Rohrdanz, K. M. Martins and J. M. Herbert, The Journal of Chemical Physics **130**, 054112 (2009).
84. D. Mester and M. Kállay, J. Chem. Theory Comput. **18**, 1646-1662 (2022).
85. P.-F. Loos, M. Comin, X. Blase and D. Jacquemin, J. Chem. Theory Comput. **17**, 3666-3686 (2021).
86. R. Baer, E. Livshits and U. Salzner, in *Annual Review of Physical Chemistry, Vol 61*, edited by S. R. Leone, P. S. Cremer, J. T. Groves, M. A. Johnson and G. Richmond (2010), Vol. 61, pp. 85-109.
87. S. Kummel, Advanced Energy Materials **7**, 1700440 (2017).
88. P. Dev, S. Agrawal and N. J. English, Journal of Chemical Physics **136** (2012).
89. A. Dreuw, J. L. Weisman and M. Head-Gordon, Journal of Chemical Physics **119**, 2943-2946 (2003).
90. C. M. Isborn, B. D. Mar, B. F. E. Curchod, I. Tavernelli and T. J. Martinez, Journal of Physical Chemistry B **117**, 12189-12201 (2013).
91. M. J. G. Peach, P. Benfield, T. Helgaker and D. J. Tozer, Journal of Chemical Physics **128**, 044118 (2008).
92. A. D. Becke, The Journal of Chemical Physics **98**, 1372-1377 (1993).
93. J. Schirmer, Physical Review A **26**, 2395-2416 (1982).
94. O. Christiansen, H. Koch and P. Jørgensen, Chemical Physics Letters **243**, 409-418 (1995).
95. Y. Wang, P. Verma, L. J. Zhang, Y. Q. Li, Z. H. Liu, D. G. Truhlar and X. He, Proceedings of the National Academy of Sciences of the United States of America **117**, 2294-2301 (2020).
96. N. Mardirossian and M. Head-Gordon, Physical Chemistry Chemical Physics **16**, 9904-9924 (2014).
97. R. Peverati and D. G. Truhlar, J. Chem. Phys. **135**, 191102 (2011).
98. C. Angeli, R. Cimiraglia, S. Evangelisti, T. Leininger and J.-P. Malrieu, The Journal of Chemical Physics **114**, 10252-10264 (2001).
99. R. Pandharkar, M. R. Hermes, D. G. Truhlar and L. Gagliardi, The Journal of Physical Chemistry Letters **11**, 10158-10163 (2020).
100. D. S. King, M. R. Hermes, D. G. Truhlar and L. Gagliardi, J. Chem. Theory Comput. **18**, 6065-6076 (2022).
101. A. K. Dutta, F. Neese and R. Izsák, The Journal of Chemical Physics **145**, 034102 (2016).
102. A. K. Dutta, M. Saitow, B. Demoulin, F. Neese and R. Izsák, The Journal of Chemical Physics **150**, 164123 (2019).
103. A. K. Dutta, M. Saitow, C. Riplinger, F. Neese and R. Izsák, The Journal of Chemical Physics **148**, 244101 (2018).
104. A. Ceulemans, W. Oldenhof, C. Gorller-Walrand and L. G. Vanquickenborne, Journal of the American Chemical Society **108**, 1155-1163 (1986).
105. M. Gouterman, Journal of Molecular Spectroscopy **6**, 138-163 (1961).
106. X. K. Chen, D. Kim and J. L. Bredas, Accounts of Chemical Research **51**, 2215-2224 (2018).
107. Y. Z. Shi, H. Wu, K. Wang, J. Yu, X. M. Ou and X. H. Zhang, Chemical Science **13**, 3625-3651 (2022).

108. K. Shizu and H. Kaji, Communications Chemistry **5**, 53 (2022).
109. S. M. Suresh, D. Hall, D. Beljonne, Y. Olivier and E. Zysman-Colman, Advanced Functional Materials **30**, 1908677 (2020).
110. X. Yin, Y. He, X. Wang, Z. X. Wu, E. B. Pang, J. Xu and J. A. Wang, Frontiers in Chemistry **8**, 725 (2020).
111. E. Goll, M. Ernst, F. Moegle-Hofacker and H. Stoll, The Journal of Chemical Physics **130**, 234112 (2009).